

MM-LDM: Multi-Modal Latent Diffusion Model for Sounding Video Generation

Mingzhen Sun
Institute of Automation,
Chinese Academy of
Science
School of Artificial
Intelligence, University of
Chinese Academy of
Sciences
Beijing, China
sunmingzhen2020@ia.ac.cn

Weining Wang
Institute of Automation,
Chinese Academy of
Science
School of Artificial
Intelligence, University of
Chinese Academy of
Sciences
Beijing, China
weining.wang@nlpr.ia.ac.cn

Yanyuan Qiao
University of Adelaide
Adelaide, Australia
yanyuan.qiao@adelaide.edu.au

Jiahui Sun
Institute of Automation,
Chinese Academy of
Science
School of Artificial
Intelligence, University of
Chinese Academy of
Sciences
Beijing, China
sunjiahui19@mails.ucas.ac.cn

Zihan Qin
Institute of Automation,
Chinese Academy of
Science
School of Artificial
Intelligence, University of
Chinese Academy of
Sciences
Beijing, China
qinzihan2021@ia.ac.cn

Longteng Guo
Institute of Automation,
Chinese Academy of
Science
School of Artificial
Intelligence, University of
Chinese Academy of
Sciences
Beijing, China
longteng.guo@nlpr.ia.ac.cn

Xinxin Zhu
Institute of Automation,
Chinese Academy of
Science
School of Artificial
Intelligence, University of
Chinese Academy of
Sciences
Beijing, China
xinxin.zhu@nlpr.ia.ac.cn

Jing Liu*
Institute of Automation,
Chinese Academy of
Science
School of Artificial
Intelligence, University of
Chinese Academy of
Sciences
Beijing, China
jliu@nlpr.ia.ac.cn

ABSTRACT

Sounding Video Generation (SVG) is an audio-video joint generation task challenged by high-dimensional signal spaces, distinct data formats, and different patterns of content information. To address these issues, we introduce a novel multi-modal latent diffusion model (MM-LDM)¹ for the SVG task. We first unify the representation of audio and video data by converting them into a single or a couple of images. Then, we introduce a hierarchical multi-modal autoencoder that constructs a low-level perceptual latent space for each modality and a shared high-level semantic feature space. The former space is perceptually equivalent to the raw signal space of each modality but drastically reduces signal dimensions. The latter space serves to bridge the information gap between modalities and provides more insightful cross-modal guidance. Our proposed method achieves new state-of-the-art results with significant quality and efficiency gains. Specifically, our method achieves a comprehensive improvement on all evaluation metrics and a faster training and sampling speed on Landscape and AIST++ datasets. Moreover,

we explore its performance on open-domain sounding video generation, long sounding video generation, audio continuation, video continuation, and conditional single-modal generation tasks for a comprehensive evaluation, where our MM-LDM demonstrates exciting adaptability and generalization ability.

CCS CONCEPTS

• **Computing methodologies** → *Hierarchical representations*; Neural networks; **Computer vision tasks**.

KEYWORDS

Multi-modal Generation, Sounding Video Generation, Latent Diffusion Model, Audio Generation, Video Generation

ACM Reference Format:

Mingzhen Sun, Weining Wang, Yanyuan Qiao, Jiahui Sun, Zihan Qin, Longteng Guo, Xinxin Zhu, and Jing Liu. 2024. MM-LDM: Multi-Modal Latent Diffusion Model for Sounding Video Generation. In *Proceedings of the 32nd ACM International Conference on Multimedia (MM '24)*, October 28–November 1, 2024, Melbourne, VIC, Australia. ACM, New York, NY, USA, 9 pages. <https://doi.org/10.1145/3664647.3680889>

*Corresponding author

¹Our codes will be released in <https://github.com/iva-mzsun/MM-LDM>.

Permission to make digital or hard copies of part or all of this work for personal or classroom use is granted without fee provided that copies are not made or distributed for profit or commercial advantage and that copies bear this notice and the full citation on the first page. Copyrights for third-party components of this work must be honored. For all other uses, contact the owner/author(s).

MM '24, October 28–November 1, 2024, Melbourne, VIC, Australia

© 2024 Copyright held by the owner/author(s).

ACM ISBN 979-8-4007-0686-8/24/10.

<https://doi.org/10.1145/3664647.3680889>

1 INTRODUCTION

Sound Video Generation (SVG) is an emerging task in the field of multi-modal generation, which aims to integrate auditory and visual signals for audio-video joint generation [17, 32, 33]. The integrated sounding videos closely simulate real-life video formats, providing immersive audiovisual narratives [2, 31, 37]. The potential applications of SVG span multiple fields, including film production, virtual reality, etc, making it an area worth exploring in depth.

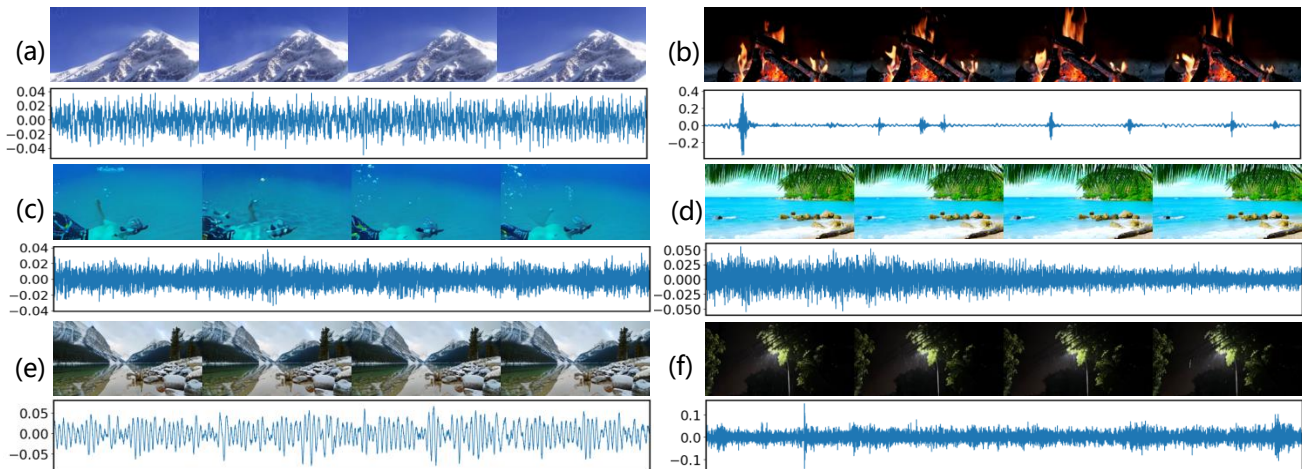


Figure 1: Sounding videos generated by our MM-LDM on the Landscape dataset [14]. We can observe vivid scenes like (a) mountain, (c) diving man, (e) lake, and so on. Matched audios are given like the sound of (b) wood burning, (d) sea wave, (f) raining, and so on. All presented audios (in this paper) can be played in Adobe Acrobat by clicking corresponding wave figures. More playable sounding video samples can be found in <https://iva-mzsun.github.io/MM-LDM>.

SVG is a challenging task that requires a deep understanding of the complex interactions between auditory and visual content [23]. Three primary challenges hinder its progress. **First**, both video and audio are high-dimensional data, making it difficult to achieve realistic generation of both modalities, especially with limited computational resources. **Second**, video and audio data have distinct dimensions and representations, necessitating specified designs to obtain a unified architecture. In particular, audios are 1D continuous auditory signals with a single amplitude channel, which focus on temporal information, whereas videos are 3D visual signals with RGB color channels, which involve both spatial and temporal information. Previous work [23] unifies video and audio generation using random-shift based attention layers, but with a small cross-modal attention window, limiting cross-modal communication and obtaining suboptimal cross-modal consistency. **Third**, patterns of content information conveyed by videos and audio are distinct. Videos record dense visual dynamics that evolve over time, while audios record sound waves made by both various visible and invisible sources. Such distinction poses a formidable challenge for current generative models to understand high-level semantic information of both modalities and generate consistent audios and videos.

To address the above challenges, we propose a novel Multi-Modal Latent Diffusion Model (MM-LDM) for SVG. Firstly, to reduce the dimension of video and audio data, we introduce a multi-modal auto-encoder that constructs two perceptual latent spaces, which are modal-specific, low-dimensional, and perceptually equivalent to the raw signal spaces. By modeling SVG within the perceptual latent spaces, we significantly reduce the computation burden and improve the generation efficiency.

Secondly, to facilitate the design of a unified framework that processes both modalities, we unify the dimensions and representations of video and audio data by encoding audio signals into an audio image and treating video signals as a sequence of images

(i.e., video frames). Such unified representation allows our multi-modal auto-encoder to utilize a pretrained image diffusion model as the signal decoder and share its parameters for both modalities. Moreover, we can explicitly model the temporal alignment of two modalities within the perceptual latent space since the perceptual latents are perceptually equivalent to raw signals, thus enabling better temporal alignment, superior synthesis quality, and improved coherence throughout the generated sample.

Thirdly, to bridge the gap between content information conveyed by two modalities, we strengthen the modeling of multi-modal correlations in both decoding and generation processes. During the decoding process, we derive a shared semantic space based on the perceptual latents to provide cross-modal guidance. Specifically, two projectors are used to map the perceptual latents into the shared semantic space. Moreover, we introduce two multi-modal semantic losses including a classification loss and a contrastive loss to optimize the high-level semantic features during training. During the generation process, we model both single-modal and cross-modal correlations using full attention. In particular, a full self-attention based Transformer [19, 27, 36] is used as the backbone of the diffusion model. It takes rasterized and concatenated audio and video perceptual latents as inputs, building both single-modal and cross-modal correlations using multiple self-attention layers.

To the best of our knowledge, MM-LDM is the first latent diffusion model for the SVG task, which requires audio-video joint generation. We introduce multiple specialized designs tailored for this multi-modal generation task as specified above. Furthermore, our proposed method exhibits remarkable adaptability when extended to various other multi-modal generation tasks, including open-domain sounding video generation, audio-to-video generation, video-to-audio generation, long sounding video generation, audio continuation, video continuation, and so on. As shown in Fig. 1, MM-LDM can synthesize high-resolution (256^2) sounding videos with vivid objects, realistic scenes, coherent motions, and aligned audio-video content. We conduct extensive experiments on

the Landscape [14], AIST++ [15], and AudioSet [5] datasets, achieving new state-of-the-art generation performance with significant visual and auditory gains. For example, on the AIST++ dataset with 256^2 spatial resolution, our MM-LDM outperforms MM-Diffusion by 114.6 FVD, 21.2 KVD, and 2.1 FAD. We also reduce substantial computational complexity, achieving a 10x faster sampling speed and allowing a larger sampling batch size. Our contributions can be summarized as follows:

- We propose a novel multi-modal latent diffusion model that establishes low-dimensional audio and video latent spaces for SVG, which are perceptually equivalent to the original signal spaces but significantly reduce the computational complexity.
- We derive a shared high-level semantic feature space from the low-level perceptual latent spaces to provide cross-modal guidance and bridge the information gap between audio-video content during the decoding process.
- We introduce multiple cross-modal losses to improve cross-modal consistency and optimize the semantic feature space, including an audio-video adversarial loss, an audio-video contrastive loss, and a classification loss.
- We perform a comprehensive evaluation and extend our method to multiple other generation tasks, which demonstrates the effectiveness, efficiency, and adaptability of our proposed method, where we achieve new state-of-the-art results with significant quality and efficiency gains.

2 RELATED WORK

Sounding Video Generation. In recent years, several works have explored the challenging task of SVG using generative adversarial networks and sequential generative models such as HMMD [13] and UVG [17]. However, their performances are far from expectations. Drawing inspiration from the success of diffusion models [9, 29], many works have explored multi-modal diffusion models for audio-video generation [23, 33, 37], while most methods focus on generating one modality based on another [18, 30, 33, 37]. Recently, MM-Diffusion [23] stands out as the pioneer in simultaneously synthesizing both modalities. To align generated audio and video content, MM-Diffusion introduces a random-shift based attention for cross-modal communication. However, this method suffers from a huge computational burden since it addresses SVG in the signal space, and uses a limited attention window size (typically no more than 8), resulting in sub-optimal cross-modal consistency. Contrastively, we establish low-level latent spaces to reduce computational complexity and a high-level latent space to provide cross-modal guidance. Our method significantly outperforms MM-Diffusion in terms of both generation efficiency and quality.

Latent Diffusion Model. Given that raw signal spaces are of high dimensions, extensive efforts have been devoted to modeling the generation of image, audio, and video modalities using latent diffusion models such as LDM [22], AudioLDM [16], and VideoLDM [1]. Most previous latent diffusion models [1, 6, 16, 22, 34] were primarily designed to encode a single modality, thus incorporating a single perceptual latent space. In contrast, our MM-LDM introduces a hierarchical multi-modal autoencoder that establishes both

low-level perceptual latent spaces and a high-level semantic feature space. The former reduces computational complexity, while the latter enhances the consistency of generated audio-video content. Such hierarchical spaces contribute to the enhanced ability to address the challenging multi-modal generation task.

3 METHOD

In this section, we present our multi-modal latent diffusion model (MM-LDM) in detail. This approach consists of two main components: a hierarchical multi-modal autoencoder designed for compressing video and audio signals, and a multi-modal latent diffusion model for modeling SVG within latent spaces. An overview of MM-LDM is shown in Fig. 2

3.1 Hierarchical Multi-Modal Autoencoder

As shown in Fig. 2 and Fig. 3, the autoencoder is composed of two modal-specific encoders, two signal decoders with shared parameters, two projectors mapping from each perceptual latent space to the shared semantic feature space, and two heads for classification and contrastive learning, respectively. Notably, our multi-modal autoencoder establishes two hierarchical feature spaces: a perceptual latent space that aligns with raw signals, and a semantic feature space derived from the perceptual space for bridging the information gap between audio and video modalities.

Unifying Representation of Video and Audio Signals. We employ the raw video signals v and transformed audio images a to be our inputs. Video $v \in \mathbb{R}^{F \times 3 \times H \times W}$ can be viewed as a sequence of 2D images (i.e. video frames), where F , 3, H , and W are video length, dimension, height, and width, respectively. Given that raw audio signals are 1D-long continuous data, we transform raw audio signals into 2D audio images to reduce computation complexity and unify the representation of audio and video inputs. In particular, given a raw audio clip, we first obtain its Mel Spectrogram with values normalized, which is denoted as $a_{raw} \in \mathbb{R}^{D \times T}$, where D represents the number of audio channels and T is the temporal dimension. Notably, a_{raw} can be transformed to raw 1D audio signals using pretrained HiFiGAN [11]. Then, we treat a_{raw} as a grayscale image and convert it into an RGB image using the PIL Python toolkit. Finally, we resize the image to the same spatial resolution as the video input, obtaining an audio image $a \in \mathbb{R}^{3 \times H \times W}$.

Modal-specific Perceptual Latent Spaces. Given a pair of audio and video inputs, we employ a pretrained KL-VAE [22] to down-sample the video frames and audio images by a factor of f . Then, as depicted in Fig. 3(a), we introduce an audio encoder to compress the audio image into $z_a \in \mathbb{R}^{C \times H_a \times W_a}$, which further downsamples the audio image by a factor of f_a , where C is the number of channels, H_a and W_a denotes $\frac{H}{f \times f_a}$ and $\frac{W}{f \times f_a}$, respectively. Similarly, the video encoder compresses video frames into $z_v \in \mathbb{R}^{C \times H_v \times W_v}$. The video encoder requires additional temporal layers to capture temporal correlations between video frames. Moreover, pixel distributions of audio images and video frames differ greatly since audio images are typical images in physics that depict wave features while video frames record real-life object appearances. Based on the above insights, parameters of the audio and video encoder are not shared and their perceptual latent spaces are modal-specific.

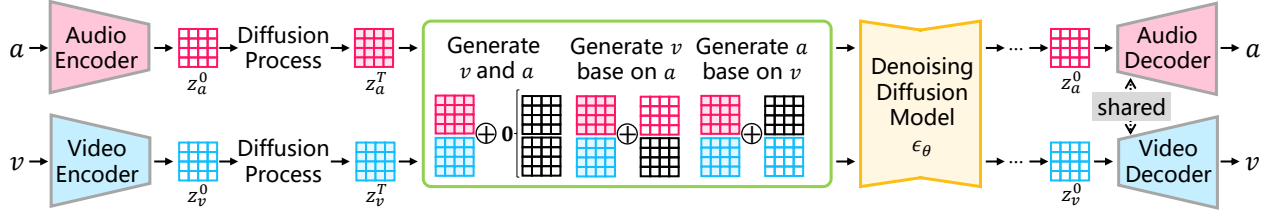


Figure 2: Overall illustration of our multi-modal latent diffusion model (MM-LDM) framework. Modules with gray border comprise our hierarchical multi-modal autoencoder. The module with orange border is our transformer-based diffusion model that performs SVG in the latent space. The green rectangle depicts the modification of inputs for unconditional audio-video generation (i.e. SVG), audio-to-video generation, and video-to-audio generation, respectively.

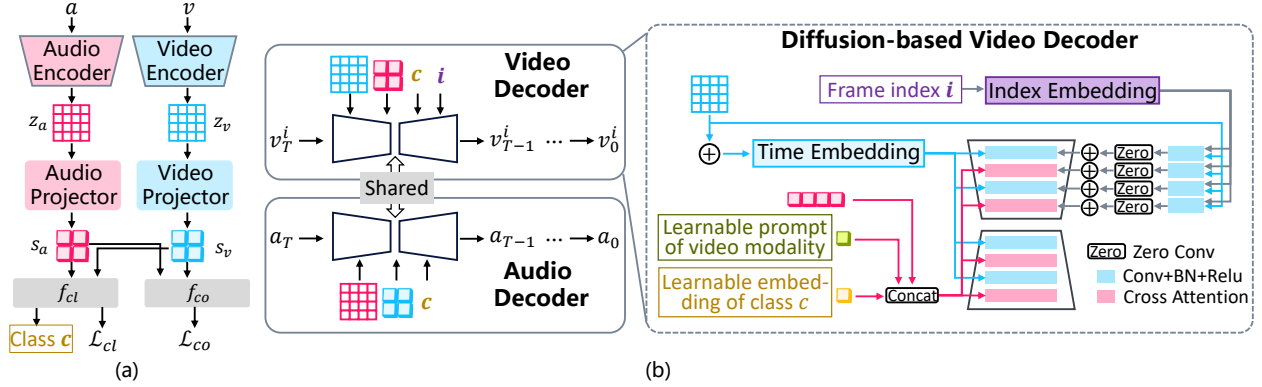


Figure 3: The detailed architecture of our multi-modal autoencoder. (a) Given audio and video inputs, two modal-specific encoders learn their perceptual latents. Two projectors map from two respective perceptual latent spaces to the shared semantic space. \mathcal{L}_{cl} represents the classification loss and \mathcal{L}_{co} denotes the contrastive loss. (b) We share the decoder parameters and incorporate multiple conditional information for signal decoding. For the video modality, we provide a specific input of frame index to extract information of the target video frame.

A Shared High-level Semantic Space. In our experiments, we observe a significant performance drop when we directly use one perceptual latent as condition input to provide cross-modal information when decoding another perceptual latent. This performance drop reveals that it is hard for the signal decoder to extract useful cross-modal information from perceptual latent features. This can be mainly attributed to the fact that perceptual latents are dense representations of low-level information, thus presenting challenges for the decoder to comprehend. To provide the decoder with useful cross-modal guidance, as depicted in Fig. 3(a), we introduce an audio projector and a video projector that establish a shared high-level semantic space based on the low-level perceptual latents. In particular, the audio and video projectors extract semantic audio and video features s_a and s_v from their perceptual latents. To ensure the extracted features are of high-level semantic information, we employ a classification head f_{cl} that takes a pair of audio and video features as inputs and predicts its class label, which is optimized using a classification cross-entropy loss. A contrastive loss is employed with a specified contrastive head to bridge the gap between video and audio features. The contrastive head f_{co} maps s_a and s_v to 1D features respectively and calculates their contrastive loss with matched pairs of audio-video features being positive samples and all unmatched pairs of audio-video features as negative samples.

Following [20], we define the contrastive loss as follows:

$$\mathcal{L}_{co} = -\frac{1}{2} \sum_{i=1}^B \log \frac{\exp(\tau \cdot \text{sim}(f_{co}(s_a^i), f_{co}(s_v^i)))}{\sum_{j=1}^B \exp(\tau \cdot \text{sim}(f_{co}(s_a^i), f_{co}(s_v^j)))} - \frac{1}{2} \sum_{i=1}^B \log \frac{\exp(\tau \cdot \text{sim}(f_{co}(s_v^i), f_{co}(s_a^i)))}{\sum_{j=1}^B \exp(\tau \cdot \text{sim}(f_{co}(s_v^i), f_{co}(s_a^j)))} \quad (1)$$

where $\text{sim}(\ast)$ calculates the dot product of input features, B and τ denote the batch size and a learnable parameter, respectively.

Signal Decoding. As illustrated in Fig. 3(b), during the reconstruction of video signals, the signal decoder takes into consideration multiple factors, including the video perceptual latent z_v , frame index i , audio semantic feature s_a , learnable modality embedding, and learnable class embedding. The video perceptual latent feature plays a critical role by imposing strict constraints from two perspectives. First, for a dense spatial constraint, frame-specific multi-scale features are extracted from the latent feature using residual blocks and added to the outputs of the UNet encoder. These features encompass detailed spatial information for the i -th video frame. Second, to provide comprehensive global instruction, a content feature is derived by pooling the latent feature across spatial channels. This content feature is then added to the time embedding. The audio semantic features are rasterized and concatenated with the learnable modality embedding and the class embedding. This concatenated

feature is then fed into cross-attention layers to provide rich conditional information. When dealing with audio reconstruction, the signal decoder employs similar inputs, excluding the frame index. More details can be found in the supplementary material.

Training Targets. Following [7], we utilize the ϵ -prediction to optimize our signal decoder, which involves the noise mean square error loss \mathcal{L}_{MSE} . Following [22], we incorporate additional KL losses \mathcal{L}_{KL}^a and \mathcal{L}_{KL}^v to punish the distributions of audio and video latents towards an isotropic Gaussian distribution. Previous works have proven the effectiveness of adversarial loss in training single-modal autoencoders [3, 25]. Here, we introduce a novel adversarial loss to improve the quality of reconstructed multi-modal signals in terms of both single-modal realism and multi-modal consistency. We first obtain a pair of decoded video frames $\langle \bar{v}_i, \bar{v}_j \rangle$ with $i < j$ and corresponding audio image \bar{a} . Then, for the optimization of the discriminator, we select $\langle a, v_i, v_j \rangle$ as the real sample and $\langle \bar{a}, \bar{v}_i, \bar{v}_j \rangle$, $\langle \bar{a}, \bar{v}_i, v_j \rangle$, $\langle \bar{a}, v_i, \bar{v}_j \rangle$, and $\langle \bar{a}, \bar{v}_i, \bar{v}_i \rangle$ to be the fake samples. $\langle \bar{a}, \bar{v}_i, \bar{v}_j \rangle$ is viewed as the real sample for our autoencoder. Our adversarial loss can be formulated as \mathcal{L}_{GAN}^D for the discriminator and \mathcal{L}_{GAN}^{AE} for our autoencoder:

$$\begin{aligned} \mathcal{L}_{GAN}^D = & \log(1 - \mathcal{D}(\langle a, v_i, v_j \rangle)) + \log \mathcal{D}(\langle \bar{a}, \bar{v}_i, \bar{v}_j \rangle) \\ & + \log \mathcal{D}(\langle \bar{a}, \bar{v}_i, v_j \rangle) + \log \mathcal{D}(\langle \bar{a}, v_i, \bar{v}_j \rangle) \\ & + \log \mathcal{D}(\langle \bar{a}, \bar{v}_i, \bar{v}_i \rangle) \end{aligned} \quad (2)$$

$$\mathcal{L}_{GAN}^{AE} = \log(1 - \mathcal{D}(\langle \bar{a}, \bar{v}_i, \bar{v}_j \rangle))$$

Our discriminator is constructed by several spatio-temporal modules that consist of residual blocks and cross-modal full attentions. Our final training loss for the multi-modal autoencoder becomes:

$$\begin{aligned} \mathcal{L}_{AE} = & \mathcal{L}_{MSE} + \lambda_{cl} \mathcal{L}_{cl} + \lambda_{co} \mathcal{L}_{co} \\ & + \lambda_{kl} (\mathcal{L}_{KL}^a + \mathcal{L}_{KL}^v) + \lambda_{gan} \mathcal{L}_{GAN}^{AE} \end{aligned} \quad (3)$$

where λ_{cl} , λ_{co} , λ_{kl} and λ_{gan} are predefined hyper-parameters. \mathcal{L}_{cl} and \mathcal{L}_{co} are the classification and contrastive losses, respectively.

3.2 Multi-Modal Latent Diffusion Model

As illustrated in Fig. 2, our approach independently corrupts audio and video latents during the forward diffusion process, whereas in the reverse denoising diffusion process, we employ a unified model that jointly predicts noise for both modalities. In particular, during forward diffusion, we corrupt audio and video latents, which are denoted as z_a^0 and z_v^0 (i.e. z_a and z_v), by T steps using a shared transition kernel. For simplicity, we use z^0 to represent both z_a^0 and z_v^0 in the subsequent section. Following prior works [7, 23], we define the transition probabilities as follows:

$$q(z^t | z^{t-1}) = \mathcal{N}(z^t; \sqrt{1 - \beta_t} z^{t-1}, \beta_t \mathbf{I}) \quad (4)$$

$$q(z^t | z^0) = \mathcal{N}(z^t; \sqrt{\bar{\alpha}_t} z^0, (1 - \bar{\alpha}_t) \mathbf{I}) \quad (5)$$

where $\{\beta_t \in (0, 1)\}_{t=1}^T$ is a set of shared hyper-parameters, $\alpha_t = 1 - \beta_t$, and $\bar{\alpha}_t = \prod_{i=1}^t \alpha_i$. Utilizing Eq. (5), we obtain corrupted latents z^t at time step t as follows:

$$z^t = \sqrt{\bar{\alpha}_t} z^0 + (1 - \bar{\alpha}_t) n^t \quad (6)$$

where $n^t \sim \mathcal{N}(0, \mathbf{I})$ represents noise features n_a^t and n_v^t for z_a^t and z_v^t respectively. The reverse diffusion processes of audio and video latents $q(z^{t-1} | z^t, z^0)$ have theoretically traceable distributions. To

capture correlations between audio and video modalities, we introduce a unified denoising diffusion model θ . This model takes both corrupted audio and video latents (z_a^t, z_v^t) as input and jointly predicts their noise features. The reverse diffusion process of corrupted audio and video latents is formulated as:

$$q((z_a^{t-1}, z_v^{t-1}) | (z_a^t, z_v^t)) = \mathcal{N}((z_a^{t-1}, z_v^{t-1}) | \mu_\theta(z_a^t, z_v^t), \tilde{\beta}_t \mathbf{I}) \quad (7)$$

During training, we minimize the mean square error between the predicted and original noise features of matched audio-video pairs, known as ϵ -prediction in the literature [10]:

$$\mathcal{L}_\theta = \frac{1}{2} \|\tilde{n}_\theta^a(z_a^t, z_v^t, t) - n_a^t\|_2 + \frac{1}{2} \|\tilde{n}_\theta^v(z_a^t, z_v^t, t) - n_v^t\|_2 \quad (8)$$

Here, $\tilde{n}_\theta^a(z_a^t, z_v^t, t)$ and $\tilde{n}_\theta^v(z_a^t, z_v^t, t)$ are the predicted audio and video noise features, respectively. Given that our audio and video latent features z_a and z_v possess relatively small spatial resolution, we employ a Transformer-based diffusion model known as DiT [19] as our backbone model. We rasterize audio and video latent features and independently add positional embeddings [28] to each latent. Then, two learnable token embeddings, $[EOS_a]$ and $[EOS_v]$, are defined and inserted before the audio and video features, respectively. Finally, audio and video latent features are concatenated and fed to DiT for multi-modal generation.

3.3 Conditional Generation

Inspired by the classifier-free guidance [8, 21, 24], we employ a cross-modal sampling guidance that targets both audio-to-video and video-to-audio generation tasks. Our approach involves training the single MM-LDM to simultaneously learn three distributions: $\tilde{n}_\theta(z_a^t, z_v^t, t)$, $\tilde{n}_\theta(z_v^t, t; z_a)$, and $\tilde{n}_\theta(z_a^t, t; z_v)$, corresponding to the SVG, audio-to-video and video-to-audio generation tasks respectively. To accomplish this, we incorporate a pair of null audio and video latents, defined as $(\mathbf{0}_a, \mathbf{0}_v)$ with $\mathbf{0}_a = 0$ and $\mathbf{0}_v = 0$. Then, the unconditional distribution $\tilde{n}_\theta(z_a^t, z_v^t, t)$ can be reformulated to be $\tilde{n}_\theta(z_a^t, z_v^t, t; \mathbf{0}_a, \mathbf{0}_v)$. The conditional distribution $\tilde{n}_\theta(z_v^t, t; z_a)$ can be reformulated as $\tilde{n}_\theta(z_a^t, z_v^t, t; z_a, \mathbf{0}_v)$, where z_a^t can be obtained directly given z_a and t according to Eq. (6). Similarly, $\tilde{n}_\theta(z_a^t, t; z_v)$ is reformulated as $\tilde{n}_\theta(z_a^t, z_v^t, t; \mathbf{0}_a, z_v)$. As depicted in Fig. 2, the conditional inputs are added to the input latents after zero convolution layers (which are ignored in the figure for conciseness) to provide conditional information. We randomly select 5% training samples for each conditional generation task. Finally, taking audio-to-video generation as an example, we define sampling as follows:

$$\tilde{n}_\theta^v(z_v^t, t; z_a) = \phi \cdot \tilde{n}_\theta^v(z_a^t, z_v^t, t; z_a, \mathbf{0}_v) - (1 - \phi) \cdot \tilde{n}_\theta^v(z_a^t, z_v^t, t; \mathbf{0}_a, \mathbf{0}_v) \quad (9)$$

where ϕ serves as a hyper-parameter that controls the intensity of the conditioning.

4 EXPERIMENT

4.1 Experimental Setups

Following [23], we conduct experiments on three popular sounding video datasets, namely Landscape [14], AIST++ [15], and AudioSet [5]. For video evaluation, we follow previous settings [4, 23, 35] that employ the Fréchet Video Distance (FVD) and Kernel Video Distance (KVD) metrics for video evaluation and Fréchet Audio Distance (FAD) for audio evaluation. Our MM-LDM synthesizes all

Table 1: Quantitative comparison on tasks of 1) v: video generation, 2) a: audio generation, 3) svg: sounding video generation, 4) a2v: audio-to-video, and 5) v2a: video-to-audio generation. Results with * are reproduced using released sources.

Method	Resolution	Sampler	Landscape			AIST++		
			FVD ↓	KVD ↓	FAD ↓	FVD ↓	KVD ↓	FAD ↓
Ground Truth	64 ²	-	16.3	-0.015	7.7	6.8	-0.015	8.4
Ground Truth	256 ²	-	22.4	0.128	7.7	11.5	0.043	8.4
Single-Modal Video Generation								
DIGAN [35]	64 ²	-	305.4	19.6	-	119.5	35.8	-
TATS-base [4]	64 ²	-	600.3	51.5	-	267.2	41.6	-
MM-Diffusion-v	64 ²	dpm-solver	238.3	15.1	-	184.5	33.9	-
MM-Diffusion-v*	64 ²	dpm-solver	237.9	13.9	-	163.1	28.9	-
MM-Diffusion-v+SR*	64 ²	dpm-solver+DDIM	225.4	13.3	-	142.9	24.9	-
MM-LDM-v	64 ²	DDIM	122.1	6.4	-	83.1	13.1	-
MM-Diffusion-v+SR*	256 ²	dpm-solver+DDIM	347.9	27.8	-	225.1	51.9	-
MM-LDM-v	256 ²	DDIM	156.1	13.0	-	120.9	26.5	-
Single-Modal Audio Generation								
Diffwave [12]	-	-	-	-	14.0	-	-	15.8
MM-Diffusion-a	-	dpm-solver	-	-	13.6	-	-	13.3
MM-Diffusion-a*	-	dpm-solver	-	-	9.6	-	-	12.6
MM-LDM-a	-	DDIM	-	-	10.7	-	-	11.7
Multi-Modal Generation								
MM-Diffusion-svg	64 ²	DDPM	117.2	5.8	10.7	75.7	11.5	10.7
MM-Diffusion-svg	64 ²	dpm-solver	229.1	13.3	9.4	176.6	31.9	12.9
MM-Diffusion-svg+SR*	64 ²	dpm-solver+DDIM	211.2	12.6	9.9	137.4	24.2	12.3
MM-LDM-a2v	64 ²	DDIM	89.2	4.2	-	71.0	10.8	-
MM-LDM-v2a	-	DDIM	-	-	9.2	-	-	10.2
MM-LDM-svg	64 ²	DDIM	77.4	3.2	9.1	55.9	8.2	10.2
MM-Diffusion-svg+SR*	256 ²	dpm-solver+DDIM	332.1	26.6	9.9	219.6	49.1	12.3
MM-LDM-a2v	256 ²	DDIM	123.1	10.4	-	128.5	33.2	-
MM-LDM-svg	256 ²	DDIM	105.0	8.3	9.1	105.0	27.9	10.2

Table 2: Efficiency comparison with MM-Diffusion [23] on a V100 32G GPU, which models SVG within the signal space. MBS denotes the Maximum Batch Size.

Method	HW	Training		Inference	
		MBS	Time/Step	MBS	Time/Sample
MM-Diffusion	64 ²	4	1.70s	32	33.1s
MM-Diffusion	128 ²	1	2.36s	16	90.0s
MM-LDM (ours)	256 ²	9	0.46s	4	70.7s
MM-LDM* (ours)	256 ²	12	0.38s	33	8.7s

Table 3: Human Evaluation on the Landscape dataset.

Method	AQ↑	VQ↑	A-V↑
MM-Diffusion	2.46	2.10	2.99
MM-LDM	2.98	3.68	3.29

videos at a 256² resolution. We resize the synthesized videos when testing the metrics in the 64² resolution.

When training our multi-modal autoencoder, we utilize pre-trained KL-VAE [22] with the downsample factor being 8. Both video frames and audio images are resized to a 256² resolution, and video clips have a fixed length of 16 frames ($F = 16$). The audio and video encoders use downsample factors of $f_a = 4$ and $f_v = 2$, yielding latents of spatial size 8² and 16², respectively. The number of latent channels is 16 for both modalities. The loss weights λ_{cl} , λ_{co} , and λ_{gan} are 1e-1, 1e-1, and 1e-1, respectively. The loss weight λ_{kl} is set as 1e-9 for Landscape and 1e-8 for AIST++. Further details can be found in the supplementary material.

4.2 Quantitative Comparison

Quality. We quantitatively compare our method with prior works for single-modal generation (i.e. video or audio generation) and multi-modal audio-video joint generation (i.e. audio-to-video, video-to-audio, and sounding video generation) tasks. The results are reported in Table. 1. For the single-modal generation tasks like audio generation and video generation, our MM-LDM outperforms MM-Diffusion by 191.8 FVD, 14.8 KVD and 104.2 FVD, 25.4 KVD at 256² resolution on Landscape and AIST++ datasets, respectively. These results reveal the potential of our MM-LDM in modeling audio and video generation tasks. For multi-modal joint generation, we report the performance of MM-LDM on audio-to-video, video-to-audio, and sounding video generation tasks. It can be observed that MM-LDM synthesizes better video results with conditional audio inputs than non-conditions, and so for audio generation. This phenomenon demonstrates that our MM-LDM can capture insightful cross-modal information to assist the generation of a single modality. For sounding video generation at the 64² resolution, we achieve a 39.8 FVD, 2.6 KVD and 1.6 FAD improvement on the Landscape dataset and a 19.8 FVD, 3.3 KVD and 0.5 FAD improvement on the AIST++ dataset compared to MM-Diffusion. At the 256² resolution, we achieve a 227.1 FVD, 18.3 KVD, and 0.8 FAD improvement on the Landscape dataset and a 114.6 FVD, 21.2 KVD and 2.1 FAD improvement on the AIST++ dataset. It can be seen that our method enhances the generation quality more significantly

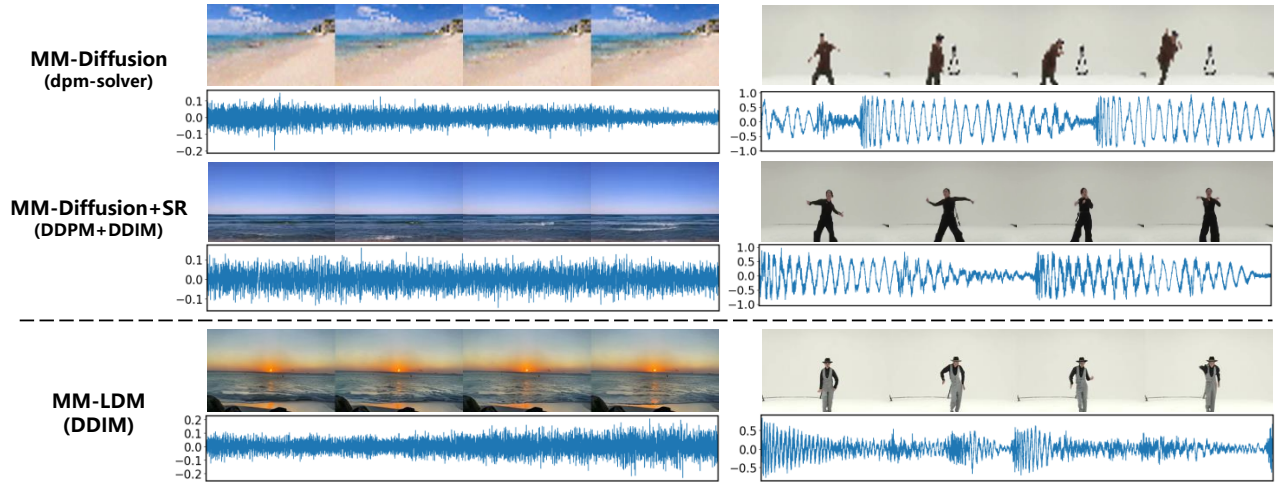


Figure 4: Qualitative comparison of sounding video samples: MM-Diffusion vs. MM-LDM (ours). All presented audios can be played in Adobe Acrobat by clicking corresponding wave figures.

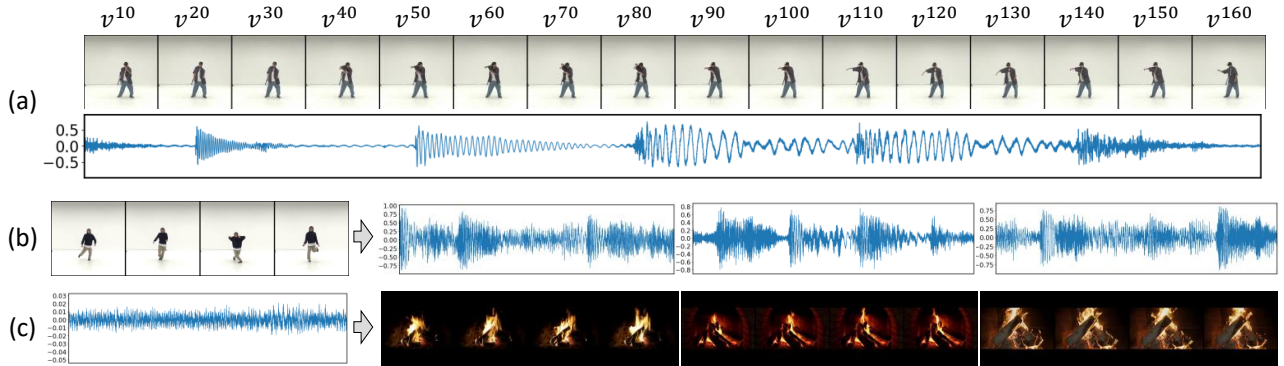


Figure 5: Samples of (a) long sounding video generation, (b) video-to-audio generation, and (c) audio-to-video generation tasks.

when the resolution increases, demonstrating the necessity of perceptual latent spaces for high-resolution sounding video generation. Notably, when using the DDPM sampler, MM-Diffusion requires 1000 diffusion steps to synthesize a sounding video sample, while our MM-LDM synthesizes higher-resolution videos with only 50 sampling steps using the DDIM sampler.

Efficiency. We quantitatively compare the efficiency of our MM-LDM and MM-Diffusion and present the results in Table. 2. MM-LDM incorporates both the auto-encoder and the DiT generator, while MM-LDM* only tests the DiT generation performance by pre-processing and saving all latents. We fix the batch size being 2 when testing the one-step time during training and the one sample time during inference, and DDIM sampler is used with 50 steps for both methods. Since MM-Diffusion operates in the signal space, it demands huge computational complexity when the spatial resolution of synthesized videos increases. In particular, it struggles to model high-resolution (256^2) video signals on a 32G V100, leading to the out-of-memory error. We evaluate the efficiency of MM-Diffusion with two spatial resolution settings: 64^2 and 128^2 . MM-LDM demonstrates improved efficiency with higher video resolutions (256^2 vs.

128^2) during the training process. When employing the same batch size (i.e., 2), our MM-LDM outperforms MM-Diffusion by 6x speed for each training step, allowing a larger training batch size with a higher video resolution. During inference, our diffusion generative model DiT, which performs SVG within the latent space, achieves a 10x faster sampling speed and allows a larger sampling batch size.

4.3 Human Evaluation

For a thorough assessment, we conduct a manual evaluation of videos sampled by both MM-Diffusion and our MM-LDM on the landscape dataset. We randomly synthesize 500 sounding video samples using each model, obtaining a total of 1000 samples. These samples are then divided into five groups, with each group consisting of 200 samples for user rating. Following MM-Diffusion [23], each video is evaluated from three perspectives: audio quality (AQ), video quality (VQ), and audio-video matching (A-V), corresponding to sounding clarity, visual realism, and audio-video alignment, respectively. Each rating has a maximum score of 5. Each group of samples are shuffled and delivered to two users for voting. The average scores are shown in Table 3. Our MM-LDM significantly

Table 4: Quantitative comparison with scaled-up data and model for open-domain generation.

Model	Params	FLOPS	FVD ↓	KVD ↓	FAD ↓
MM-Diffusion [23]	134M	567G	649.8	34.6	2.9
MM-LDM-S	131M	34G	185.8	10.1	1.59
MM-LDM-B	384M	101G	181.5	9.5	1.55
MM-LDM-L	1543M	407G	164.1	8.5	1.52

Table 5: Ablation study on the multi-modal autoencoder on the Landscape dataset.

Model	rFVD ↓	rKVD ↓	rFAD ↓
MM-LDM	53.9	2.4	8.9
–Adversarial training loss	75.7	3.9	8.9
–Finetune KL-VAE decoder	80.1	4.3	9.1
–Semantic cross-modal feature	87.7	5.1	9.1
–Learnable class embedding	94.4	5.7	9.2
–Latent average pooling	105.5	6.8	9.0
–Learnable modality prompt	110.7	6.9	9.3
–Weight Initialization	132.4	8.1	10.7

surpasses MM-Diffusion by 0.52 AQ, 1.58 VQ, and 0.30 A-V, demonstrating the effectiveness of our proposed method and the necessity of constructing multi-modal latent space.

4.4 Qualitative Comparison

We qualitatively compare the generative performance of our MM-LDM and MM-Diffusion in Fig. 4, using the provided checkpoints of MM-Diffusion when sampling. Videos synthesized by MM-Diffusion produce blurry appearances with deficient details, whereas our MM-LDM yields clearer samples with better audio-video alignments.

To further explore the adaptivity of our proposed method, we extend it to the long sounding video generation task in an auto-regressive manner, which is specified in the supplementary material. We present the sample of long sounding video generation in Fig. 5(a), where our method can synthesize realistic and coherent long sounding videos with up to 160 frames. We also test the generation performance on conditional single-modal generation tasks like video-to-audio generation and audio-to-video generation tasks. As shown in Fig. 5(b) and Fig. 5(c), our method can generate consistent and diverse audio or video samples based on the video or audio condition. We also extend our method to other generation tasks like audio continuation and video continuation and provide samples in the supplementary material.

4.5 Generalization and Scaling Capability

To explore the generalization and scaling capability of our proposed MM-LDM, we conduct experiments using a larger open-domain dataset across various scales. Specifically, similar to MM-Diffusion, we filter 100K high-quality videos from the open-domain dataset AudioSet [5]. Then we optimize both MM-Diffusion and our MM-LDM on this dataset, testing the performance of MM-LDM at three different scales, i.e., small (S), base (B), and large (L). Each experiment is conducted on 8 A800 GPUs with comparable training times. As reported in Table 4, MM-LDM significantly outperformed MM-Diffusion. Furthermore, as the number of parameters of MM-LDM increases, the performance exhibits a significant boost, revealing the potential of our proposed method in terms of scaling capability. Samples of open-domain video generation are provided in the supplementary material.

Table 6: Sensitivity analysis on loss weights.

# Reso.	λ_{kl}	λ_{co}	λ_{cl}	rFVD 64 ²	rKVD 64 ²	rFAD 64 ²	rFVD 256 ²	rKVD 256 ²	rFAD 256 ²
1	1e-8	1.0	1.0	68.0	11.2	10.0	89.7	23.8	10.0
2	1e-8	0.3	0.3	62.6	10.8	10.0	90.3	24.5	9.9
3	1e-8	0.1	0.1	59.6	10.4	9.8	85.1	21.4	9.9
4	1e-7	0.1	0.1	63.5	10.7	10.0	88.8	24.2	10.0

4.6 Ablation Studies

We conduct ablation studies on our multi-modal autoencoder and report the results in Table. 5. Our base autoencoder independently decodes signals for each modality based on the respective spatial information from perceptual latents. To reduce computational complexity, we share the diffusion-based signal decoder for both modalities and initialize its parameters with [22]. Two learnable embeddings are incorporated to prompt each modality. For a more comprehensive content representation, we apply average pooling to each perceptual latent, adding the latent feature to the timestep embedding and further enhancing the model performance. By incorporating the classification and contrastive losses, we leverage prior knowledge of class labels and extract high-level cross-modal information, which significantly boosts model performance. Since the KL-VAE was originally trained on natural images and is unfamiliar with physical images like audio images, we finetune its decoder on each dataset for better performance. Finally, after training with the adversarial loss, our autoencoder attains its best reconstruction performance, achieving 53.9 rFVD, 2.4 rKVD, and 8.9 rFAD.

4.7 Sensitivity Analysis

Following prior work [26], we consistently utilized an adversarial learning weight of 0.1 in all experiments. In addition, we experimented with four configurations of loss weights, each obtained after a 20-epoch run (approximately 16K steps) on the AIST++ dataset. Across different settings, we assess metrics such as FVD, KVD, and FAD for samples at resolutions of 64 and 256. As reported in Table 6, where Reso. denotes resolution, the performance of configuration #3 outperforms that of other configurations at both 64² and 256² resolutions. Thus, we select configuration #3 as the default configuration in this paper.

5 CONCLUSION

This paper introduces MM-LDM, a novel latent diffusion model for the SVG task. To reduce the computational complexity, we establish a low-level perceptual latent space for each modality, which is perceptually equivalent to the raw signal space but encompasses a much smaller feature size. Moreover, we employ a dual safeguard mechanism to ensure cross-modal consistency between generated audio and video content. First, we derive a high-level semantic space to provide more insightful cross-modal information when decoding audio and video latents. Second, sufficient cross-modal communication is allowed during the generation progress by incorporating a full-attention mechanism into generative models. Our method achieves new state-of-the-art results on multiple benchmarks with improved efficiency and exciting adaptability.

ACKNOWLEDGMENTS

This work was supported by the Key Research and Development Program of Jiangsu Province under Grant BE2023016-3, the National Science and Technology Major Project (NO. 2023ZD0121201), National Natural Science Foundation of China (62102416, 62102419).

REFERENCES

- [1] Andreas Blattmann, Robin Rombach, Huan Ling, Tim Dockhorn, Seung Wook Kim, Sanja Fidler, and Karsten Kreis. 2023. Align your latents: High-resolution video synthesis with latent diffusion models. In *Proceedings of the IEEE/CVF Conference on Computer Vision and Pattern Recognition*. 22563–22575.
- [2] Moitrya Chatterjee and Anoop Cherian. 2020. Sound2sight: Generating visual dynamics from sound and context. In *European Conference on Computer Vision*. 701–719.
- [3] Patrick Esser, Robin Rombach, and Bjorn Ommer. 2021. Taming transformers for high-resolution image synthesis. In *Proceedings of the IEEE/CVF Conference on Computer Vision and Pattern Recognition*. 12873–12883.
- [4] Songwei Ge, Thomas Hayes, Harry Yang, Xi Yin, Guan Pang, David Jacobs, Jia-Bin Huang, and Devi Parikh. 2022. Long video generation with time-agnostic vqgan and time-sensitive transformer. In *European Conference on Computer Vision*. 102–118.
- [5] Jort F Gemmeke, Daniel PW Ellis, Dylan Freedman, Aren Jansen, Wade Lawrence, R Channing Moore, Manoj Plakal, and Marvin Ritter. 2017. Audio set: An ontology and human-labeled dataset for audio events. In *IEEE International Conference on Acoustics, Speech and Signal Processing*. IEEE, 776–780.
- [6] Yingqing He, Tianyu Yang, Yong Zhang, Ying Shan, and Qifeng Chen. 2022. Latent video diffusion models for high-fidelity video generation with arbitrary lengths. *arXiv preprint arXiv:2211.13221* (2022).
- [7] Jonathan Ho, Ajay Jain, and Pieter Abbeel. 2020. Denoising diffusion probabilistic models. *Advances in Neural Information Processing Systems* 33 (2020), 6840–6851.
- [8] Jonathan Ho and Tim Salimans. 2022. Classifier-free diffusion guidance. *arXiv preprint arXiv:2207.12598* (2022).
- [9] Rongjie Huang, Jiawei Huang, Dongchao Yang, Yi Ren, Luping Liu, Mingze Li, Zhenhui Ye, Jinglin Liu, Xiang Yin, and Zhou Zhao. 2023. Make-An-Audio: Text-To-Audio Generation with Prompt-Enhanced Diffusion Models. In *International Conference on Machine Learning*. 13916–13932.
- [10] Diederik Kingma, Tim Salimans, Ben Poole, and Jonathan Ho. 2021. Variational diffusion models. *Advances in Neural Information Processing Systems* 34 (2021), 21696–21707.
- [11] Jungil Kong, Jaehyeon Kim, and Jaekyoung Bae. 2020. Hifi-gan: Generative adversarial networks for efficient and high fidelity speech synthesis. *Advances in Neural Information Processing Systems* 33 (2020), 17022–17033.
- [12] Zhifeng Kong, Wei Ping, Jiaji Huang, Kexin Zhao, and Bryan Catanzaro. 2021. DiffWave: A Versatile Diffusion Model for Audio Synthesis. In *International Conference on Learning Representations*.
- [13] Vinod K. Kurmi, Vipul Bajaj, Badri N. Patro, K. S. Venkatesh, Vinay P. Nambodiri, and Preethi Jyothi. 2021. Collaborative Learning to Generate Audio-Video Jointly. In *IEEE International Conference on Acoustics, Speech and Signal Processing*. 4180–4184.
- [14] Seung Hyun Lee, Gyeongrok Oh, Wonmin Byeon, Chanyoung Kim, Won Jeong Ryoo, Sang Ho Yoon, Hyunjun Cho, Jihyun Bae, Jinkyu Kim, and Sangpil Kim. 2022. Sound-guided semantic video generation. In *European Conference on Computer Vision*. 34–50.
- [15] Ruilong Li, Shan Yang, David A Ross, and Angjoo Kanazawa. 2021. Ai choreographer: Music conditioned 3d dance generation with aist++. In *Proceedings of the IEEE/CVF International Conference on Computer Vision*. 13401–13412.
- [16] Haojie Liu, Zehua Chen, Yi Yuan, Xinhao Mei, Xubo Liu, Danilo P. Mandic, Wenwu Wang, and Mark D. Plumbley. 2023. AudioLDM: Text-to-Audio Generation with Latent Diffusion Models. In *International Conference on Machine Learning*. 21450–21474.
- [17] Jiawei Liu, Weining Wang, Sihan Chen, Xinxin Zhu, and Jing Liu. 2023. Sounding Video Generator: A Unified Framework for Text-guided Sounding Video Generation. *IEEE Transactions on Multimedia* (2023), 1–13.
- [18] Simian Luo, Chuanhao Yan, Chenxu Hu, and Hang Zhao. 2024. Diff-foley: Synchronized video-to-audio synthesis with latent diffusion models. *Advances in Neural Information Processing Systems* 36 (2024).
- [19] William Peebles and Saining Xie. 2023. Scalable diffusion models with transformers. In *Proceedings of the IEEE/CVF International Conference on Computer Vision*. 4195–4205.
- [20] Alec Radford, Jong Wook Kim, Chris Hallacy, Aditya Ramesh, Gabriel Goh, Sandhini Agarwal, Girish Sastry, Amanda Askell, Pamela Mishkin, Jack Clark, et al. 2021. Learning transferable visual models from natural language supervision. In *International Conference on Machine Learning*. 8748–8763.
- [21] Aditya Ramesh, Prafulla Dhariwal, Alex Nichol, Casey Chu, and Mark Chen. 2022. Hierarchical text-conditional image generation with clip latents. *arXiv preprint arXiv:2204.06125* (2022).
- [22] Robin Rombach, Andreas Blattmann, Dominik Lorenz, Patrick Esser, and Björn Ommer. 2022. High-resolution image synthesis with latent diffusion models. In *Proceedings of the IEEE/CVF Conference on Computer Vision and Pattern Recognition*. 10684–10695.
- [23] Ludan Ruan, Yiyang Ma, Huan Yang, Huiguo He, Bei Liu, Jianlong Fu, Nicholas Jing Yuan, Qin Jin, and Baining Guo. 2023. Mm-diffusion: Learning multi-modal diffusion models for joint audio and video generation. In *Proceedings of the IEEE/CVF Conference on Computer Vision and Pattern Recognition*. 10219–10228.
- [24] Chitwan Saharia, William Chan, Saurabh Saxena, Lala Li, Jay Whang, Emily L Denton, Kamyar Ghasemipour, Raphael Gontijo Lopes, Burcu Karagol Ayan, Tim Salimans, et al. 2022. Photorealistic text-to-image diffusion models with deep language understanding. *Advances in Neural Information Processing Systems* 35 (2022), 36479–36494.
- [25] Mingzhen Sun, Weining Wang, Zihan Qin, Jiahui Sun, Sihan Chen, and Jing Liu. 2024. GLOBER: Coherent Non-autoregressive Video Generation via GLOBAL Guided Video DecodER. *Advances in Neural Information Processing Systems* 36 (2024).
- [26] Mingzhen Sun, Weining Wang, Xinxin Zhu, and Jing Liu. 2023. MOSO: Decomposing MOTion, Scene and Object for Video Prediction. In *Proceedings of the IEEE/CVF conference on Computer Vision and Pattern Recognition*. 18727–18737.
- [27] Yepeng Tang, Weining Wang, Chunjie Zhang, Jing Liu, and Yao Zhao. 2024. Learnable Feature Augmentation Framework for Temporal Action Localization. *IEEE Transactions on Image Processing* 33 (2024), 4002–4015. <https://doi.org/10.1109/TIP.2024.3413599>
- [28] Ashish Vaswani, Noam Shazeer, Niki Parmar, Jakob Uszkoreit, Llion Jones, Aidan N Gomez, Łukasz Kaiser, and Illia Polosukhin. 2017. Attention is all you need. *Advances in Neural Information Processing Systems* 30 (2017).
- [29] Ruben Villegas, Mohammad Babaeizadeh, Pieter-Jan Kindermans, Hernan Moraldo, Han Zhang, Mohammad Taghi Saffar, Santiago Castro, Julius Kunze, and Dumitru Erhan. 2023. Phenaki: Variable Length Video Generation from Open Domain Textual Descriptions. In *International Conference on Learning Representations*.
- [30] Heng Wang, Jianbo Ma, Santiago Pascual, Richard Cartwright, and Weidong Cai. 2024. V2a-mapper: A lightweight solution for vision-to-audio generation by connecting foundation models. In *Proceedings of the AAAI Conference on Artificial Intelligence*, Vol. 38. 15492–15501.
- [31] Wenxuan Wang, Quan Sun, Fan Zhang, Yepeng Tang, Jing Liu, and Xinlong Wang. 2024. Diffusion Feedback Helps CLIP See Better. *arXiv preprint arXiv:2407.20171* (2024).
- [32] Ruihan Yang, Hannes Gamper, and Sebastian Braun. 2023. CMMD: Contrastive Multi-Modal Diffusion for Video-Audio Conditional Modeling. *CoRR* abs/2312.05412 (2023).
- [33] Guy Yariv, Itai Gat, Sagie Benaim, Lior Wolf, Idan Schwartz, and Yossi Adi. 2024. Diverse and aligned audio-to-video generation via text-to-video model adaptation. In *Proceedings of the AAAI Conference on Artificial Intelligence*, Vol. 38. 6639–6647.
- [34] Sihyun Yu, Kihyuk Sohn, Subin Kim, and Jinwoo Shin. 2023. Video probabilistic diffusion models in projected latent space. In *Proceedings of the IEEE/CVF Conference on Computer Vision and Pattern Recognition*. 18456–18466.
- [35] Sihyun Yu, Jihoon Tack, Sangwoo Mo, Hyunsu Kim, Junho Kim, Jung-Woo Ha, and Jinwoo Shin. 2022. Generating Videos with Dynamics-aware Implicit Generative Adversarial Networks. In *International Conference on Learning Representations*.
- [36] Tongtian Yue, Jie Cheng, Longteng Guo, Xingyuan Dai, Zijia Zhao, Xingjian He, Gang Xiong, Yisheng Lv, and Jing Liu. 2024. SC-Tune: Unleashing Self-Consistent Referential Comprehension in Large Vision Language Models. In *Proceedings of the IEEE/CVF Conference on Computer Vision and Pattern Recognition*. 13073–13083.
- [37] Ye Zhu, Yu Wu, Kyle Olszewski, Jian Ren, Sergey Tulyakov, and Yan Yan. 2022. Discrete contrastive diffusion for cross-modal and conditional generation. *arXiv preprint arXiv:2206.07771* (2022).